# The Mechanical Nature of Stress-Corrosion Cracking in Al-Zn-Mg Alloys: I. Evaluation of the Ductile Rupture Contribution*

W. E. WOOD AND W. W. GERBERICH

A detailed study of rapid stress-corrosion-cracking (SCC) in a 7075 aluminum alloy has allowed separation of the mechanical and chemical contributions. This was accomplished by combining scanning electron microscopy, stress-wave emission and crack growth rate observations as a function of test temperature. These established an activation energy of 11.2 kcal/mol, a stress-intensity squared dependence of crack growth, and a range of 20 to 80 pct dimpled rupture on the fracture surfaces. Thus a two-step crack growth mechanism is proposed combining a thermally activated electrochemical process and a discontinuous mechanical jumping process.

THE case for the type of stress-corrosion-cracking (SCC) mechanism in aluminum alloys has oscillated between those who advocate a purely electrochemical dissolution process[1-5] and those who advocate a combined electrochemical-mechanical process.[6-9] From an electrochemical viewpoint, most explanations involve localized dissolution at anodic sites such as precipitate particles, e.g., $MgZn_2$, or emerging slip bands within the precipitate free zone (PFZ). A combined mechanism adds in some discontinuous brittle or ductile rupture process so that the overall mechanism is an alternating two-step process. A subset problem area has been whether or not the PFZ width of high-strength aluminum alloys plays a major role in the process.[10-12] Although considerable work has been done on electrochemical and PFZ aspects, there have been relatively few quantitative attempts to determine the extent of micromechanical contributions to SCC except for the theoretical model proposed by Krafft and Mulherin.[8]

The following study of 7075 aluminum was designed to attempt a detailed definition of the mechanical aspect of the SCC mechanism. First, a recrystallization treatment to aid in providing a reasonable grain-boundary path and a low pH solution were utilized to promote rapid SCC. Second, the initiation stage was eliminated by starting with a pre-fatigue cracked, edge-notched specimen. Third, crack propagation rates were determined as a function of stress intensity factor to obtain a better mechanical description of the growth process. Fourth, tests were run at a relatively constant stress intensity level as a function of test temperature to define the activation energy of

the thermally activated mechanism. Finally, a stress-wave emission (SWE) technique to monitor any discontinuous crack jumps and scanning electron microscopy were utilized to separate out mechanical and chemical contributions to the growth process.

## EXPERIMENTAL PROCEDURE

Commercially obtained 7075 aluminum alloy was first cold rolled from 0.080 to 0.060 in. in thickness and then solution heat treated at 500°C for 3 days and quenched in water at 82°C, resulting in a cooling rate of about 65°C/s.[13] The material was then aged for 5 days at 88°C to a -T6 temper which has been reported[14] as leading to an increased susceptibility to stress corrosion cracking.

To verify the properties of the as-received alloy as well as the cold worked and heat treated alloy, standard tensile tests were done. For the SCC tests, single edge notched specimens were machined with their tensile axis perpendicular to the grain orientation of the sheet. The specimen geometry selected is that given by Brown and Srawley,[15] for which the stress intensity factor may be given in terms of load, $P$, crack length, $a$, thickness, $B$, and width, $W$, by

$$K = Y \frac{Pa}{BW}^{1/2} \tag{1}$$

with $Y$ being the finite width correction factor,

$$Y = 1.99 - 0.41 (a/W) + 18.70 (a/W)^2 - 38.48 (a/W)^3 + 53.85 (a/W)^4 \tag{1a}$$

The SEN specimens were pre-fatigue cracked in a tension-tension fatigue machine at a $\Delta k$ of 13 ksi-in.$^{1/2}$ to introduce a crack in approximately 15,000 cycles.

The SCC tests were done in a 3.5 pct NaCl solution with $AlCl_3$ added to lower the pH of the solution to less than two. In order to determine the crack growth rate as a function of temperature, the NaCl + $AlCl_3$ solution was heated to a controlled temperature, and then allowed to flow slowly through a plastic tubing and past the notched area of the SEN specimen. A thermometer was inserted into the tubing close to the specimen in order to actually measure the temperature of the solution as it passed the specimen.

W. E. WOOD, formerly with the Lawrence Radiation Laboratory, Berkeley, is now Assistant Professor, Dept. of Materials Science, Oregon Graduate Center, Beaverton, Oregon 97005. W. W. GERBERICH, formerly with the Lawrence Radiation Laboratory, Berkeley, is now Associate Professor, Dept. of Chemical Eng. and Materials Science, University of Minnesota, Minneapolis, Minn.
Manuscript submitted January 8, 1973.

Elastic stress waves are caused by the discontinuous growth of a crack before catastrophic failure. By using a suitable piezoelectric transducer attached to the specimen grips, these emissions can be detected, if they are within the sensitivity range of the instrument. The stress wave emission technique developed by Hartbower et al[16-18] has been used to study the behavior of slow crack growth propagation in SEN specimens, and provides an extremely sensitive method for monitoring stress-wave emission produced by discontinuous crack growth. The complete instrumentation and test apparatus is shown schematically in Fig. 1. As the signal is the result of a very small amount of energy being released by a discontinuous crack movement, it is necessary to amplify it and to filter out extraneous noise. After the test was over, the taped signal was played back at $7\frac{1}{2}$ ips (at one-half speed and thus one-half of the highest recorded frequency), so as to be well within the frequency response of the galvanometer (5 kHz) utilized in the recording oscillograph. The resulting gain of the system comprising the charge amplifier, voltage amplifier, and the recorder amplifier of 1 to 3, was approximately 112,500.

Standard metallographic techniques were used to examine the microstructure of the as-received material in comparison to the cold worked and heat treated material. The scanning microscope (SEM) employing secondary electron emission at 25 kV was used to study the fracture surface of the specimens over a range of magnification from 200 to 20,000 times.

## EXPERIMENTAL RESULTS AND OBSERVATIONS

Typical microstructures, as shown in Fig. 2, indicate the as-received material contained about 250 grains across the thickness, or a grain width of about 12.5 microns. After cold rolling and heat treating, there were about 70 grains across the thickness or a grain width of about 22 microns. The grain length did not change between the two conditions and averaged about 100 microns. Five tensile tests each of both conditions gave the average results in Table I.

SCC tests were done at different load levels for short intervals of crack growth so that both $K$ and $da/dt$ could be determined. Due to the geometry of the SEN specimen, the stress intensity level increases and the crack grows. Thus, for these tests, the initial value, $K_0$, and the final value, $K_f$, were calculated and an average value assumed. In order that there be only a small change in the stress intensity during the test, the tests were run long enough so that there would be a relatively small amount of crack growth. This also had the advantage of allowing little time for additional corrosion of the exposed fracture surfaces. The specimens were then broken by loading at 0.13 in./min so that the amount of slow crack growth could be determined. Fig. 3 shows a log-log plot of the stress intensity versus the slow crack growth rate. The slope of the curve, determined by a least square analysis on an IBM computer, was found to be equal to 2. No crack growth was observed (after 328 min) at a stress intensity of 9250 psi-in.$^{1/2}$.

Tests were performed to determine the dependence of the slow crack growth rate on the temperature of the environment. The results are given in Table II and shown in Fig. 4 for three different stress intensity levels. Again, a least squares analysis was done to determine the best curves that could be drawn through the data points. From the equation

$$\frac{da}{dt} = Ae^{-Q/RT} \qquad [2]$$
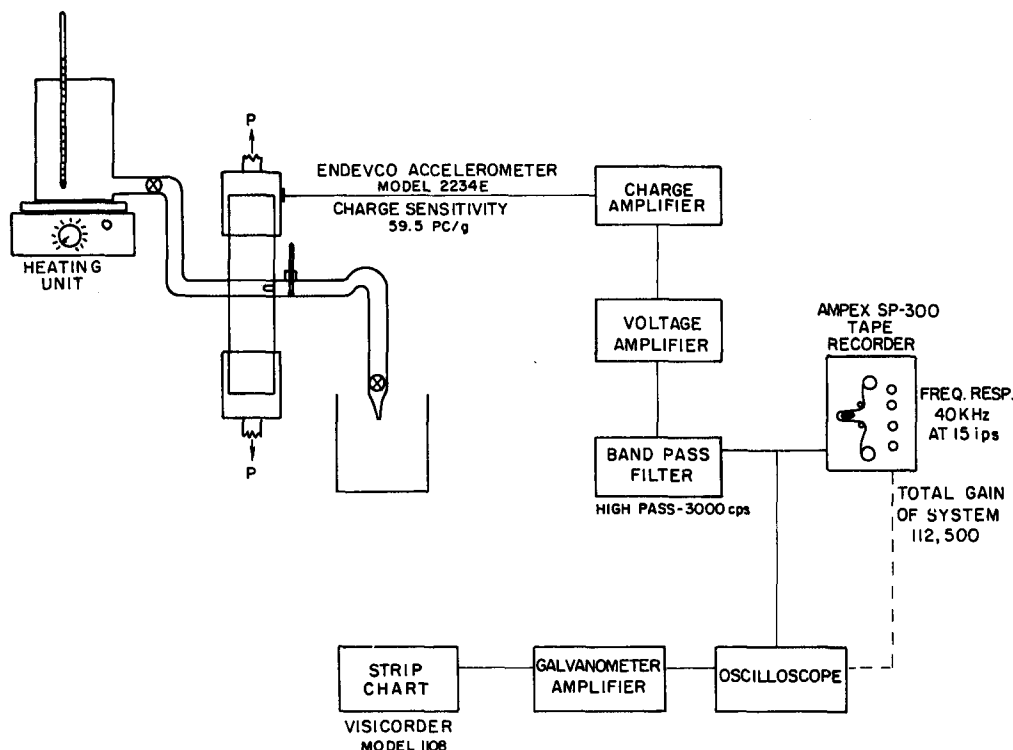
the activation energy, $Q$, can be computed from the



Fig. 1—Schematic illustration of the experimental set-up used to perform SCC tests and monitor stress wave emissions.

slope of the curves. The average value of the apparent activation energy was found to be 11.2 kcal/mol.

Stress wave activity was observed in all the tests where slow crack growth occurred. Fig. 5 shows some representative oscillogram recordings of the moni-tored waves and Table III indicates the dependence of the amplitude and frequency of the stress waves on the stress intensity. Due to the sensitivity of the system, the bubbles formed by the reaction of the environment with the material, produced a noise, which at ele-
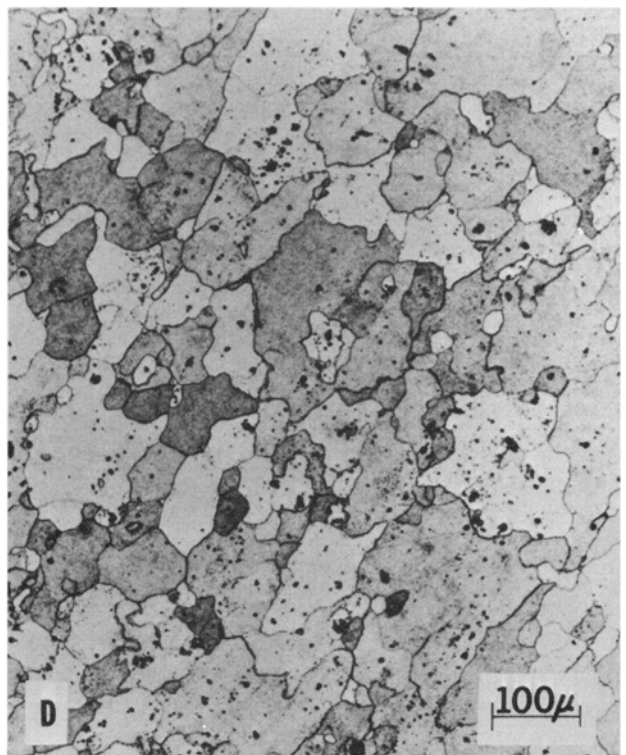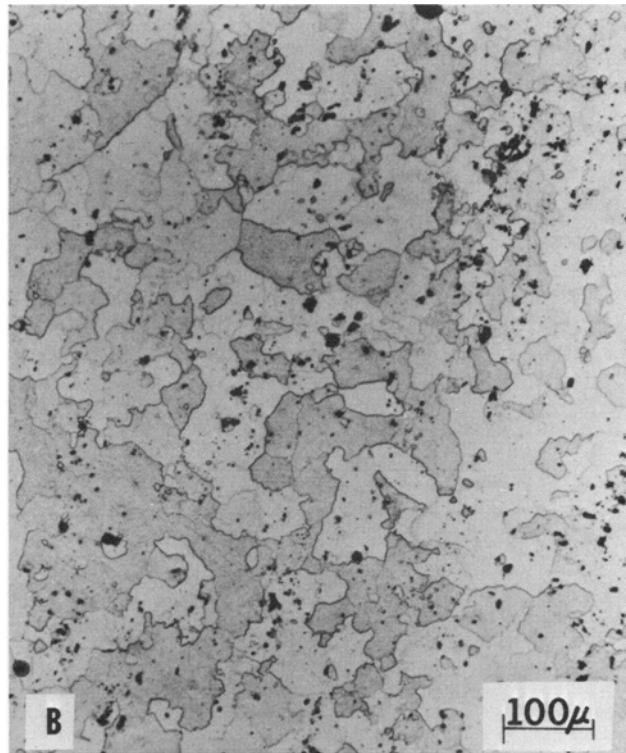


Fig. 2—Typical microstructures of 7075 aluminum sheet. (a) and (b) as received material, (c) and (d) after cold rolling from 0.080 to 0.060 in. thickness, solution heat treating and quenching. a, b viewed from the top; b, d edge view perpendicular to the rolling direction.

vated temperatures made it impossible to distinguish between real stress waves and the wave produced by the bubbles. Even at 48°C the noise of the bubbles made it impossible to identify the stress waves. However, at 33°C and below, bubbles did not significantly raise the background noise, and allowed stress waves to be observed as a function of stress intensity. For example, Fig. 5 shows that the background noise level is negligible compared to the stress waves observed during SCC tests. The number of stress waves/s taken from data stored on the tapes, is only of the major waves. The real SWE activity might possibly be somewhat higher, involving more low energy waves. The average amplitude of the stress waves for each test was obtained from the amplitude of the six biggest waves in a given time interval.

Qualitatively then, the SWE observations show that as the stress intensity increases, the frequency and amplitude of the stress waves increases. Estimates of the incremental area swept out by the crack have been made by Gerberich and Hartbower.[16] Quantitatively, a relationship between the incremental crack growth and stress wave activity has been suggested

by Gerberich and Desai.[19] Based on experimental work on an Al-Zn-Mg alloy and a theoretical compliance analysis, they derived a semi-empirical relationship of the form

$$g = \frac{2.5\,CKw^{1/2}\,\Delta A}{YBe} \qquad [3]$$

where $g$ is the amplitude of a stress wave, $\Delta A$ is the

Table I. Mechanical Properties of 7075-T6 Aluminum

| | Yield Strength (0.2 pct offset) (psi) | Ultimate Strength (psi) | pct Elong. (1.0 in. gage) | pct Reduction of area |
|---|---|---|---|---|
| As received material | 71,500 ± 1100 | 80,700 ± 400 | 11.6 ± 1.6 | 28 ± 8 |
| Rolled, solution H.T., and aged | 56,800 ± 1200 | 79,00 ± 1200 | 15.2 ± 1.8 | 26 ± 3 |

Table II. SCC Data from Crack Propagation Tests

| Test Temp. T (°C) | Stress Intensities $K_0$ (psi-in.$^{1/2}$) | $K_f$ (psi-in.$^{1/2}$) | $K_{AVE}$ (psi-in.$^{1/2}$) | Time Increment $\Delta t$ (min) | Crack Increment $\Delta a$ (in.) | Crack Growth Rate $da/dt$ (in./min) |
|---|---|---|---|---|---|---|
| 10 | 36,100 | 39,500 | 37,800 | 47.0 | .048 | .0010 |
| 23 | 45,400 | 50,700 | 48,050 | 14.8 | .070 | .0047 |
| 23 | 44,700 | 50,000 | 47,400 | 5.2 | .070 | .0135 |
| 23 | 34,700 | 38,500 | 36,600 | 19.3 | .070 | .0036 |
| 23 | 36,500 | 38,500 | 37,500 | 21.4 | .043 | .0020 |
| 23 | 32,200 | 36,800 | 35,500 | 14.7 | .055 | .0037 |
| 23 | 27,600 | 40,000 | 33,800 | 73.0 | .270 | .0037 |
| 23 | 31,700 | 34,700 | 33,200 | 25.5 | .065 | .0026 |
| 23 | 24,000 | 27,500 | 25,800 | 26.0 | .090 | .0035 |
| 23 | 23,800 | 26,300 | 25,000 | 47.0 | .077 | .0016 |
| 23 | 21,800 | 25,700 | 23,800 | 60.0 | .110 | .0018 |
| 23 | 30,600 | 52,800 | 41,700 | 67.8 | .405 | .0060 |
| 22 | 29,000 | 32,400 | 30,700 | 26.7 | .080 | .0030 |
| 23 | 14,900 | 20,500 | 17,700 | 230.0 | .195 | .00085 |
| 23 | 9,250 | 9,250 | 9,250 | 328.0 | .000 | .0000 |
| 23 | 38,900 | 39,900 | 39,400 | 13.0 | .065 | .0050 |
| 23 | 15,600 | 18,800 | 17,200 | 204.0 | .070 | .00034 |
| 32 | 46,900 | 49,900 | 48,400 | 5.2 | .045 | .0086 |
| 33 | 35,100 | 35,500 | 35,300 | 6.7 | .025 | .0037 |
| 33 | 23,800 | 25,000 | 24,400 | 7.6 | .040 | .0052 |
| 43 | 34,400 | 37,600 | 36,000 | 4.2 | .063 | .0150 |
| 43 | 25,600 | 27,500 | 26,500 | 9.4 | .050 | .0053 |
| 43 | 25,300 | 26,500 | 25,900 | 5.3 | .045 | .0085 |
| 48 | 47,700 | 51,500 | 49,600 | 1.4 | .055 | .0402 |
| 53 | 34,800 | 38,800 | 36,800 | 2.8 | .070 | .0250 |
| 53 | 24,900 | 28,500 | 26,700 | 7.5 | .090 | .0120 |
| 53 | 24,600 | 27,400 | 26,000 | 11.4 | .080 | .0070 |
| 62 | 26,200 | 25,200 | 25,700 | 0.8 | .010 | .0122 |
| 62 | 25,300 | 25,300 | 25,300 | 1.2 | .025 | .0220 |
| 68 | 47,300 | 48,700 | 48,000 | 1.1 | .076 | .0724 |
| 73 | 36,100 | 37,300 | 36,700 | 0.9 | .045 | .0500 |
| 33 | 25,500 | 25,600 | 25,550 | 1.0 | .020 | .0200 |
| 73 | 24,600 | 24,400 | 24,500 | 0.75 | .020 | .0267 |

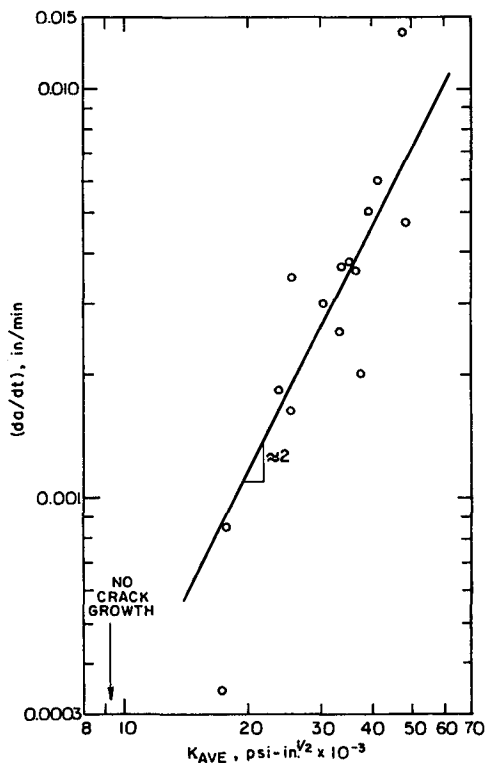Fig. 3—Stress corrosion crack growth rate vs applied stress intensity for room temperature tests of 7075-T6 aluminum.
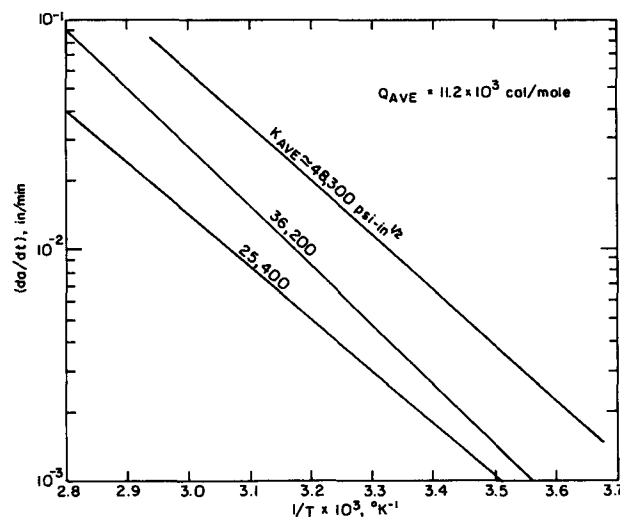
Fig. 4—Stress corrosion crack growth rates vs temperature for three levels of applied stress intensity for 7075-T6 aluminum.
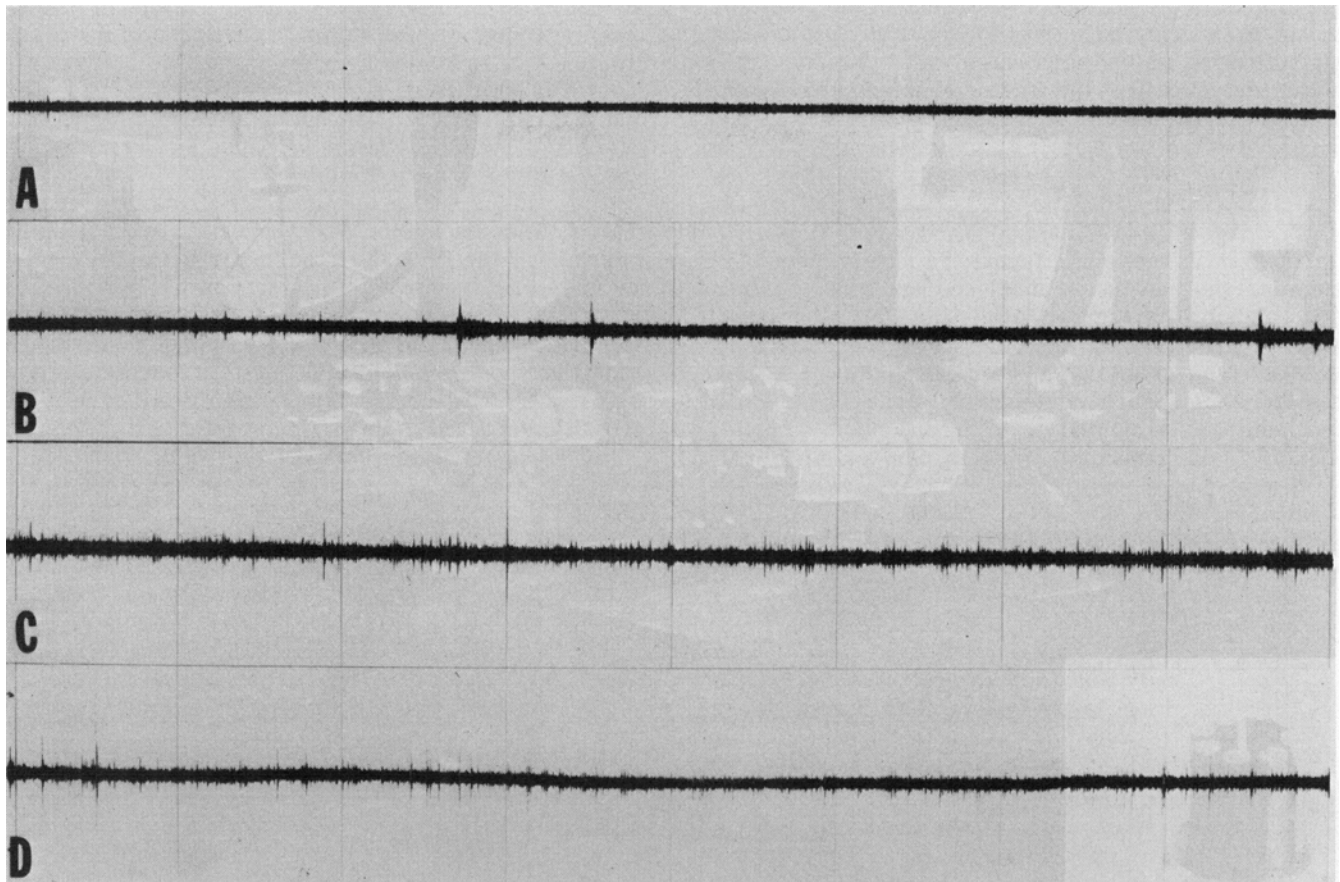
Fig. 5—Oscillogram recordings of stress waves during room temperature SCC tests of 7075 aluminum. Each frame represents 1/2 s. The stress wave amplitude represents $g$, ft/s$^2$. (a) background noise due to the testing machine and environment, no load applied, (b) SCC test with $K$ = 25,400 psi-in.$^{1/2}$, (c) SCC tests with $K$ = 36,200 psi-in.$^{1/2}$, (d) SCC test with $K$ = 48,300 psi-in.$^{1/2}$.

Table III. Stress-wave and fractographic observations

| $K_{A VE}$, psi-in.$^{1/2}$ | $T$, °C | $SWE$/s | $\Delta t_s$, s | Dimple Rupture, pct |
|---|---|---|---|---|
| 25,400 | 23 | 2.0 | 0.5 | 20 |
| 36,200 | 33 | 6.6 | 0.151 | 33 |
| 48,300 | 23 | 11.0 | 0.091 | 80 |

| $K_{A VE}$, psi-in.$^{1/2}$ | $da/dt$, in./s $\times$ 10$^5$ | SWE Amplitude, $g$, ft/s$^2$ $\times$ 10$^4$ | $\Delta A$, in.$^2$ $\times$ 10$^6$ |
|---|---|---|---|
| 25,400 | 2.7 | 2.3 | 0.078 |
| 36,200 | 10 | 3.6 | 0.085 |
| 48,300 | 12 | 5.7 | 0.113 |

incremental area swept out by a crack as associated with one stress wave, $e$ is the distance between loading pins, $C$ is a constant of about 0.05, $B$ is the specimen thickness, and $Y$ is the $f(a/w)$ appropriate to the specimen configuration. By carefully calibrating the instruments shown schematically in Fig. 1, the amplitude of the stress waves can be expressed in terms of $g$. For the settings used in these tests a stress wave amplitude of 1.9 in. is equal to 0.0008 $g$. Table III shows the calculated values of $g$ and $\Delta A$ for different stress intensity levels based on Eq. [3].

Next, consider the metallographic observations. Fig. 6 shows representative macroscopic fracture features for all the tests. Indicated on the figure is the pre-

fatigue cracked region ($a$-$b$), the slow crack growth region ($b$-$c$), and the unstable crack growth region ($c$-$d$). Figs. 7 through 10 show the microscopic details of the fracture surfaces. At low temperatures, the time of the tests was longer, and therefore the solution was in contact with the fracture surface for longer periods of time, thus destroying many of the fine details. This made it difficult to find any areas of dimpled rupture that might have been present initially. However, at high temperatures with shorter exposure times to the environment, fine detail can be observed. Fig. 7 shows the two general types of morphology observed: ($a$) a relatively flat smooth surface and ($b$) a dimpled rupture type surface. A comparison of Figs. 8 and 9 shows that as the stress intensity level increases, the amount of dimpled rupture also increases. The dimpled regions represent discontinuous jumping or tearing of the material, as compared with the relatively flat surfaces which might be indicative of electrochemical dissolution. Besides the two general characteristics of the fracture process, there were also some artifacts on the fracture surface due to fracture of precipitated salts. For example, Fig. 10($a$-$b$) clearly shows one region of a test specimen containing what seemed to be deposits of the solution. This was verified by taking the solution, drying it on a nickel plate, and examining it under the scanning electron microscope. As seen in Fig. 10($c$-$d$), the features of the residue are perfectly smooth with no texture present;

the cracks in the residue are formed as the solution dries. Comparing Fig. 10(c) to Fig. 10(b) at the same magnification strongly indicates that this feature is not characteristic of the fracture surface and is merely a result of fractured salt crystals.

## DISCUSSION

Those investigators[1-5] favoring a purely electrochemical process have considered how either matrix slip bands or a preferred slip in the PFZ might assist anodic dissolution. On the other hand, there are those[20] who have suggested that a grain-boundary crack is nucleated mechanically, and then propagates by an electrochemical mechanism or, alternatively,[21] is nucleated by an electrochemical mechanism and then prop-

agates mechanically. Various modifications of these with the influence of precipitate particles as the dissolution site have also been proposed.[14] A recent review of most of these mechanisms has been presented,[2] and thus a reiteration will not be attempted here. However, it is useful to reconsider those mechanisms with respect to the present findings.

First, one can state unequivocally from this study, that: 1) The site for the SCC process is in or at the interface of the PFZ. 2) A thermally-activated mechanism controls the rate of crack growth. 3) The crack growth rate increases with increasing stress intensity. 4) Fractographic and stress-wave emission studied show that the crack growth process is discontinuous, with mechanical rupture being a significant part of the growth mechanism.

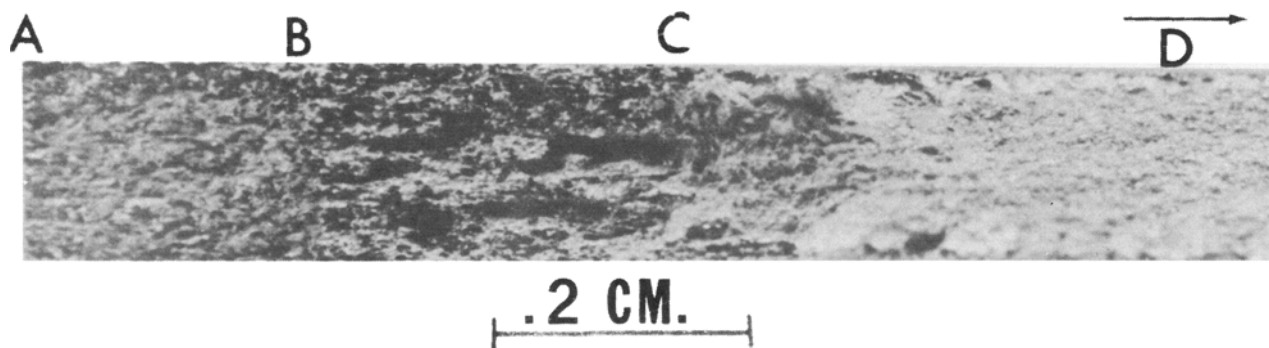All mechanisms are compatible with the first point.



Fig. 6—Macroscopic fracture features of SCC test specimen. (a-b) pre-fatigued region, (b-c) slow crack growth region, (c-d) unstable crack growth.
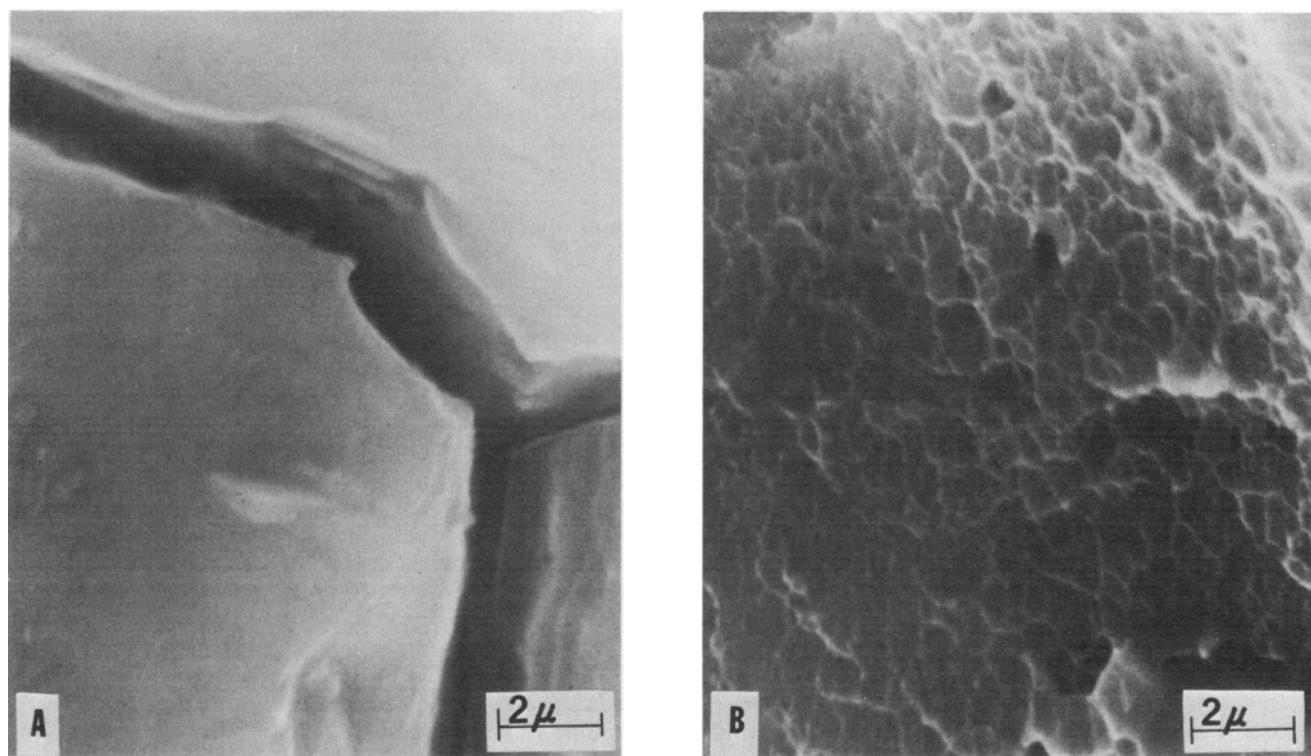


Fig. 7—Scanning electron micrographs illustrating the two different types of fracture surfaces observed in the slow crack growth regions of a SCC specimen tested at $K = 37,000$ psi-in.$^{1/2}$. (a) relatively flat fracture surface indicative of anodic dissolution, and (b) dimpled rupture fracture surface indicative of discontinuous jumping, or tearing.

The second point suggests a thermally-controlled corrosion and/or diffusion process, which is also compatible with all mechanisms. The third point would be a little difficult to understand if only an electrochemical dissolution process were involved. One could argue that with higher stress intensity factors, there are more sites, *e.g.*, greater frequency of slip bands, and hence more rapid anodic dissolution. However, in lieu of additional evidence, it is more satisfying to consider that the excess mechanical energy results in larger amounts of mechanical rupture. At least for the present investigation, the previous point is clarified by the fourth point which definitely confirms the discontinuous, mechanical feature of the SCC process.
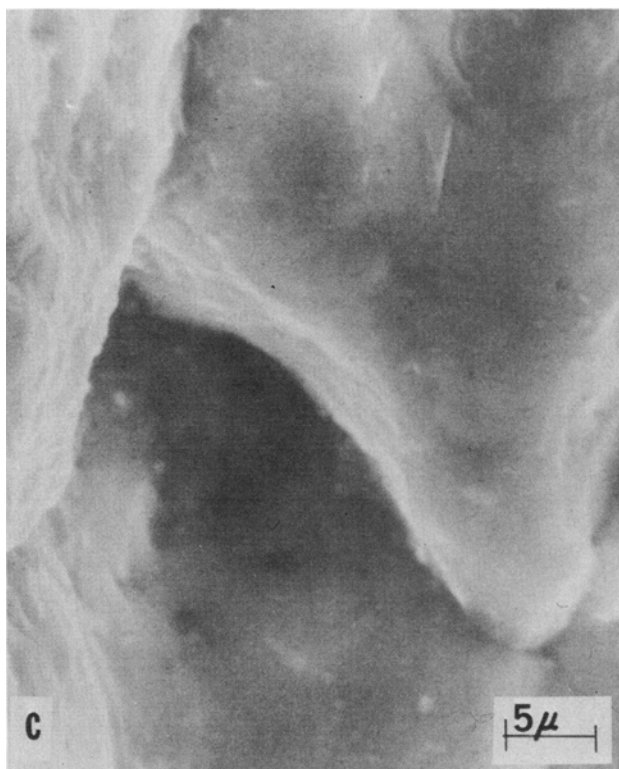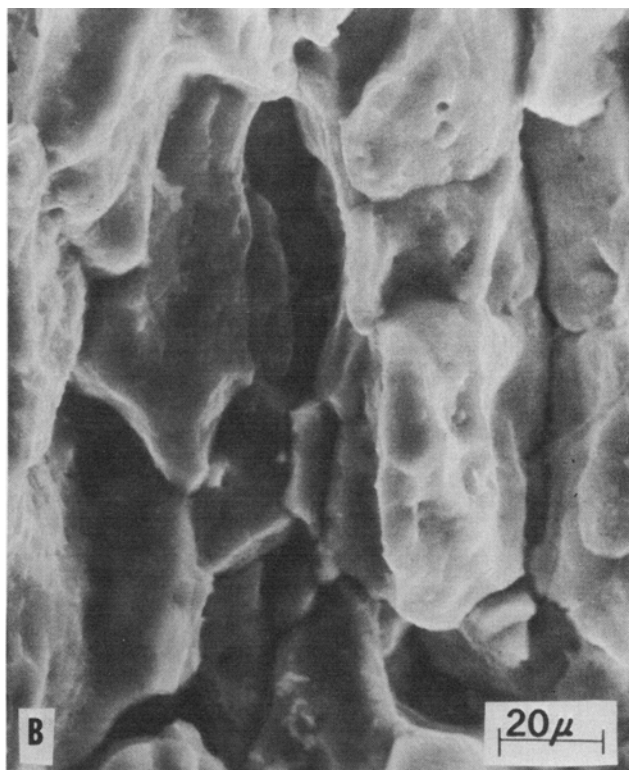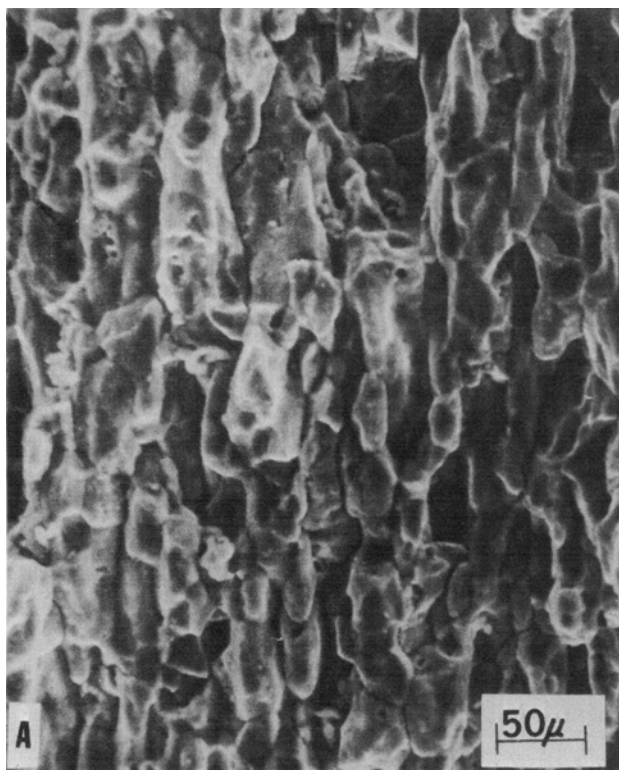


Fig. 8—Scanning electron micrographs of a SCC specimen tested at an applied stress intensity of 26,740 psi-in.$^{1/2}$.

## Mechanical Nature of the Process

In light of the present findings, it is useful to consider why the mechanical aspect of the SCC mechanism has previously been rejected. Probably the most formidable argument is that there has been little evidence on the fracture surfaces to suggest a mechanical fracture process. Jacobs[7] did report having evidence of mechanical rupture, but the corrosive nature of the "dimples" seemed to several others[22] to make this evidence inconclusive. In a similar set of experiments on a Al-Zn-Mg alloy, Sedriks, et al[10] reported no evidence of microvoid coalescence in the stress-corrosion areas. However, they did find dimpled rupture on the part of the specimen that failed by the rapid mechanical fracture that terminated the test. Even
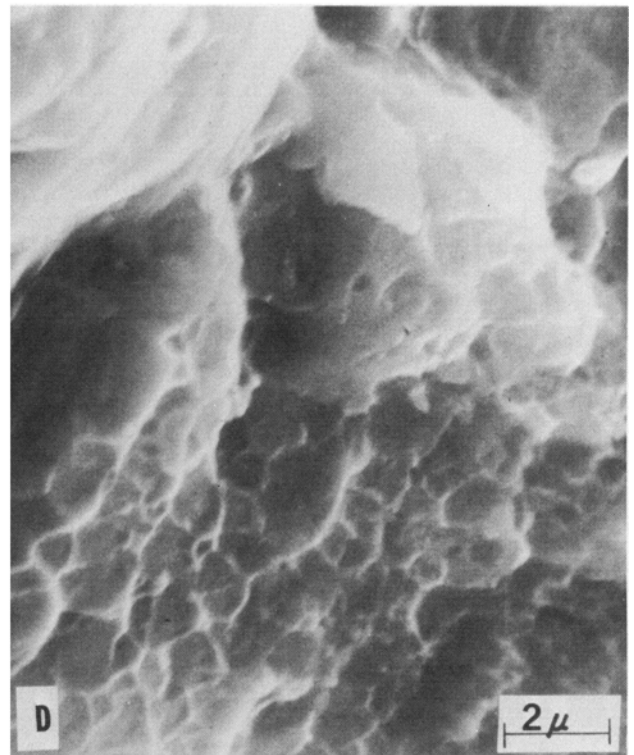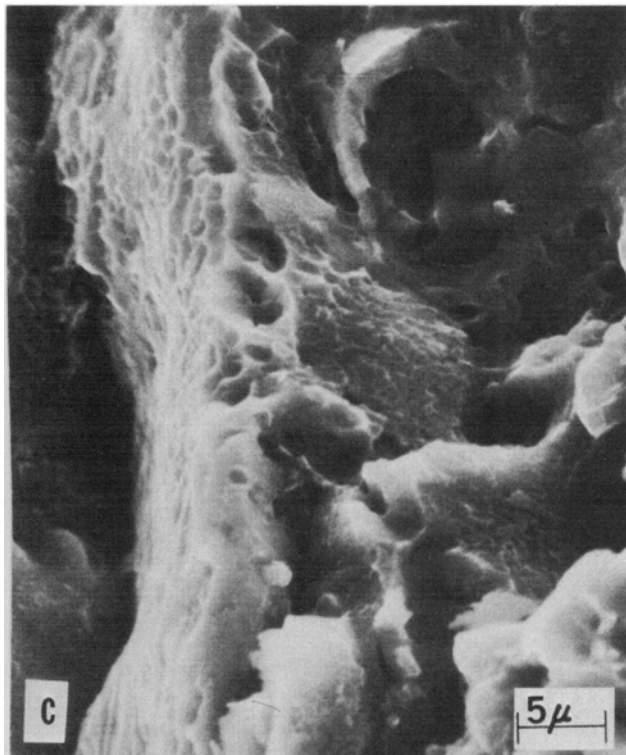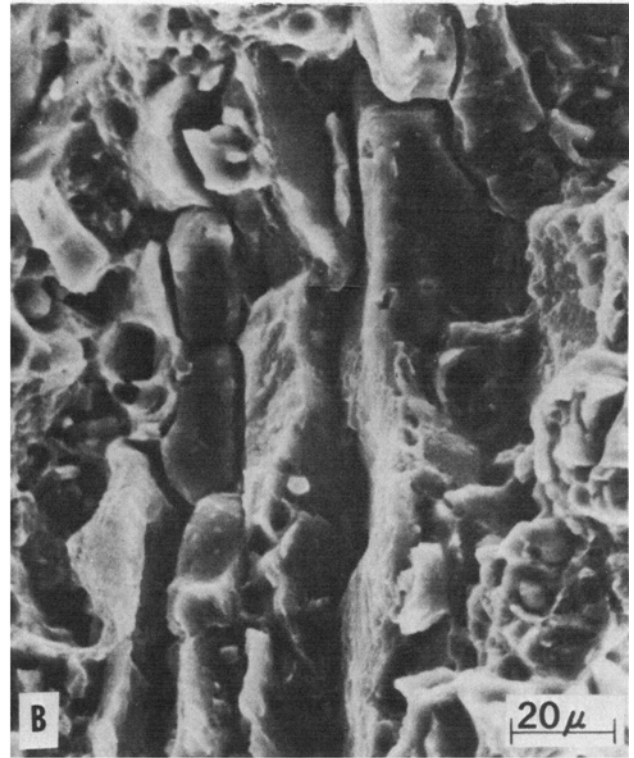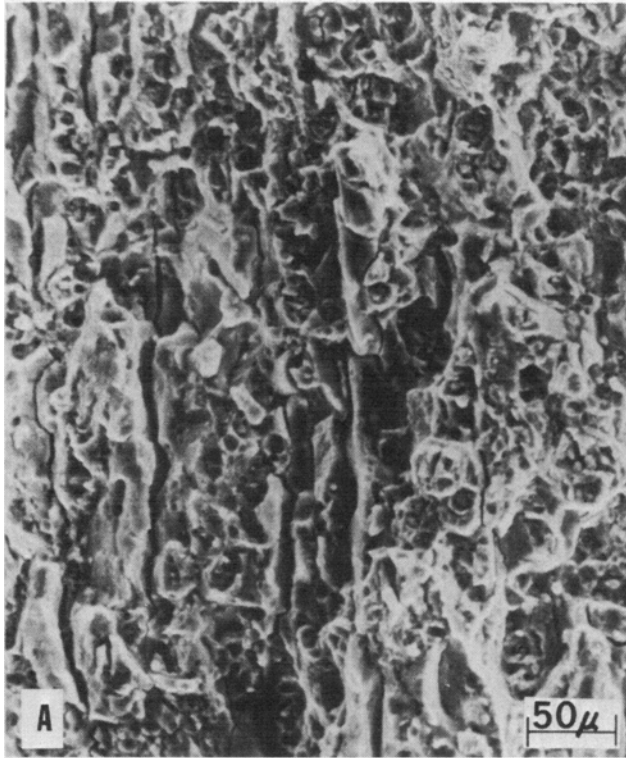


Fig. 9—Scanning electron micrographs of a SCC specimen tested at an applied stress intensity of 49,600 psi-in.$^{1/2}$.

though this rapid fracture part of the surface was exposed to the environment for some time, the dimples observed in that area were *not* attacked by corrosion. They then argued that *if* dimples existed in the SCC part of the fracture surface, these also should *not* have been corroded and hence should have been detected by either scanning electron microscopy or fractography. They therefore concluded that since no microvoids were in evidence, then the process must be purely anodic dissolution. The salient point of their argument is that the dimples forming under rapid crack growth would be as likely to corrode as dimples forming under SCC conditions, given equal time of exposure to the environment. However, there is no evidence to this effect and in fact, it is more likely that the conditions just behind a slowly growing crack would be more conducive
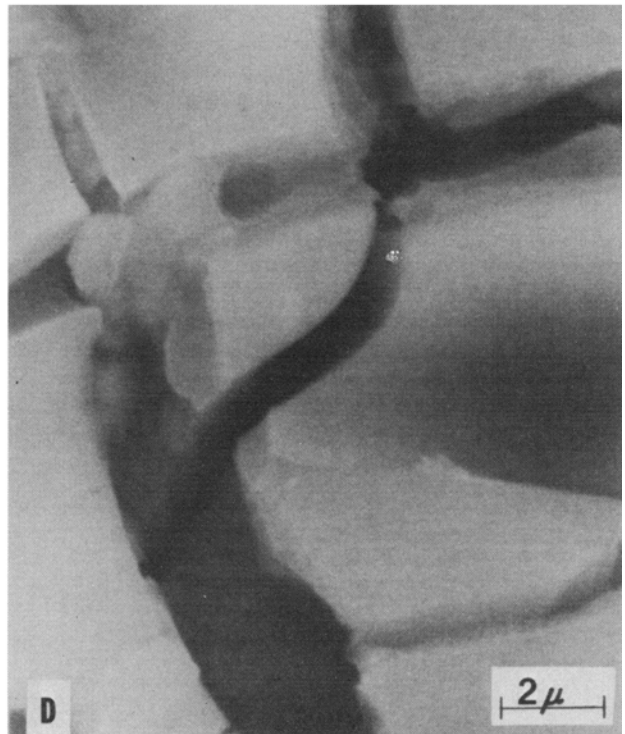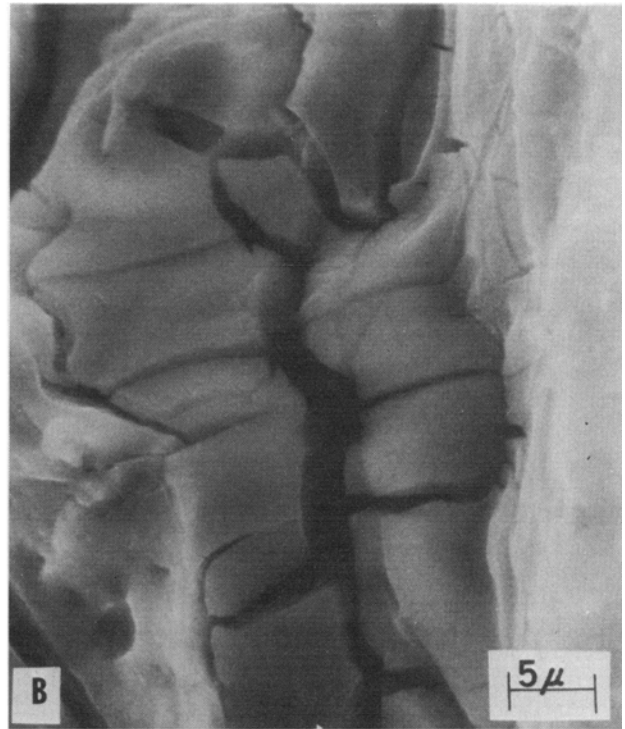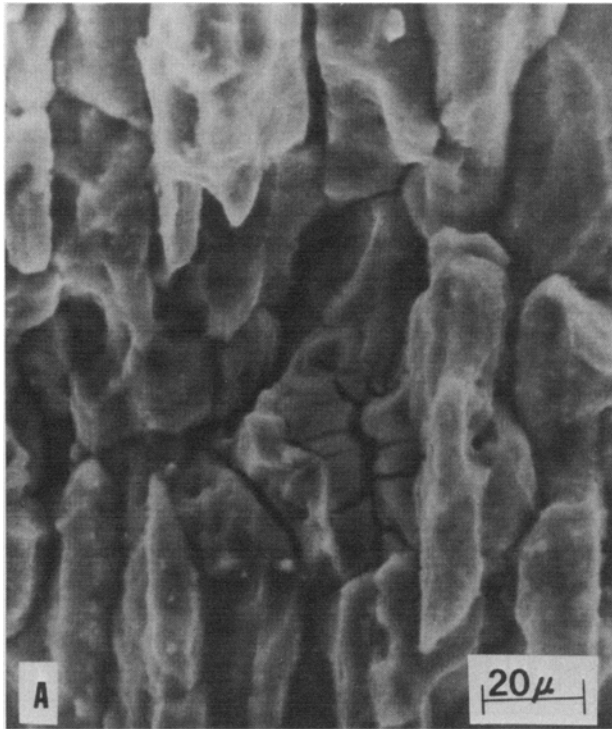


Fig. 10—Scanning electron micrograph showing a residual deposit of the test solution. (*a*) and (*b*) deposits on the actual fracture surface, and (*c*) and (*d*) deposits evaporated on a nickel plate for comparison.

to corrosion attack. Both the potential and the pH conditions would be considerably different from an unstressed, completely exposed fracture surface. Moreover, the present study has definitely established the fact that microvoid coalescence may be an integral part of the SCC mechanism in 7075-T6 aluminum. Thus, it is probable that Jacobs[7] did observe microvoid coalescence associated with SCC. The fact that the microvoids were heavily corroded suggests that in many previous cases, obliteration of the true fracture surface details may have led some investigators to conclude, erroneously, that the mechanism was entirely void of any mechanical process.

Of course, it might be argued that the present data represent a relatively unique case and that this situation is not characteristic of other aluminum alloys. However, it is significant that the crack growth rate dependence on stress intensity is nearly identical to the $K^2$ dependence observed by Tetelman and McEvily[23] for Al-5.5 Zn-2.5 Mg in a neutral NaCl solution. The only difference was that the present growth rates were faster by a factor of four. Nevertheless, this is consistent with the fact that McHardy $et$ $al$[24] reports a factor of four decrease in time to failure for 7075-T6 stressed in an NaCl + AlCl$_3$ solution where the pH is less than two as compared to a neutral NaCl solution.

One final comment about the mechanical contribution concerns the absolute magnitude of the mechanical rupture process. Consider the size of the area swept out in a single jump, as indicated by the SWE amplitude. This $0.09 \times 10^6$ in.$^2$ area would only be about 3 pct of the total cross-sectional area of a single grain. Thus, it would appear that the mechanical nature of the process, even at relatively high stress intensity levels, is a relatively localized process. This may not be so for finer grained materials or more susceptible higher strength alloys.

## CONCLUSIONS

1) The crack growth rate for the SCC process was strongly dependent on the temperature with an apparent activation energy of 11.2 kcal/mol. The crack growth rate was proportional to $K^2$.

2) Stress wave emission results showed that cracking was discontinuous and that the frequency of stress wave emissions increased with increasing stress intensity.

3) Both mechanical and electrochemical fracture in the SCC region was intergranular, and the amount of dimpled rupture was proportional to $K^2$.

4) Crack growth drying SCC is concluded to be a two-step process combining an electrochemical and mechanical process.

## CONVERSION FACTORS FOR SI UNITS

| | |
|---|---|
| 1 in. | = 2.54 cm |
| 1 micron | = $10^{-6}$ m |
| 1 kcal/mole | = 4186 J/mole |
| 1 ft/s$^2$ | = 0.3048 m/s$^2$ |
| 1 in./s | = 0.0254 m/s |
| 1 psi | = 0.01394 N/mm$^2$ |
| 1 psi-in.$^{1/2}$ | = 0.001107 MPa · m$^{1/2}$ |

## REFERENCES

1. G. Thomas and J. Nutting: *J. Inst. Metals*, 1959-60, vol. 88. p. 81.
2. D. O. Sprowls and R. H. Brown: *Proc. Conf. Fundamental Aspects of Stress Corrosion Cracking*, National Assn. of Corrosion Eng., Houston (1969), p. 446.
3. A. J. Sedriks, P. W. Slattery and E. N. Pugh: *Trans. ASM*, 1969, vol. 62, pp. 815-18.
4. F. H. Haynie and W. K. Boyd: *Proc. Conf. Fundamental Aspects of Stress Corrosion Cracking*, National Assn. of Corrosion Eng., Houston, 1969, p. 580.
5. A. J. Sedriks, J. A. S. Green, and D. L. Novak, *Met. Trans.:* 1970, vol. 1, p. 1815.
6. E. H. Dix, Jr.: *Trans. AIME*, 1940, vol. 137, p. 11.
7. A. J. Jacobs, *Proc. Conf. Fundamental Aspects of Stress Corrosion Cracking*, National Assn. of Corrosion Eng., Houston, 1969, p. 530.
8. J. M. Krafft and J. H. Mulherin: *ASM Trans. Quart.*, 1969, vol. 62, p. 64.
9. A. F. Beck and P. R. Sperry: *Proc. Conf. Fundamental Aspects of Stress Corrosion Cracking*, National Assn. of Corrosion Eng., Houston, 1969, p. 513.
10. A. J. Sedricks, P. W. Slattery, and E. N. Pugh: *ASM Trans. Quart.*, 1969, vol. 62, p. 238.
11. M. O. Speidel: *Proc. Conf. Fundamental Aspects of Stress Corrosion Cracking*, National Assn. of Corrosion Eng., Houston, 1969, p. 561.
12. P. N. T. Unwin and G. C. Smith: *J. Inst. Metals*, 1969, vol. 97, p. 299.
13. *Aluminum:* ASM, 1967, vol. 1, p. 13.
14. W. Gruhl and H. Cordier: *Z. Metalk.*, 1964, vol. 55, p. 577.
15. W. F. Brown and J. E. Srawely: *Plane Strain Crack Toughness of High Strength Materials*, ASTM, (Spec. Tech. Publ.) 410, Philadelphia, 1966.
16. W. W. Gerberich and C. E. Hartbower: *Int. J. Fracture Mec.*, 1967, vol. 3, No. 3.
17. C. E. Hartbower, W. W. Gerberich and P. P. Crimmins: *Welding J. Res. Supp.*, 1968, vol. 47, p. 433.
18. C. E. Hartbower, W. W. Gerberich, H. Liebowitz: *Eng. Frac. Mec.*, 1968, vol. 1, p. 291.
19. W. W. Gerberich and J. D. Desai: Annual Technical Progress Report I, A. E. C. Contract AT-11-1-2212, to be submitted for publication.
20. E. N. Pugh and W. P. D. Jones: *Metallurgia*, 1961, vol. 63, p. 3.
21. W. Gruhl and H. Cordier: *Trans. ASM*, 1963, vol. 56, p. 951.
22. A. J. Jacobs: *Proc. Conf. Fundamental Aspects of Stress Corrosion Cracking*, National Assn. of Corrosion Eng., Houston, 1969, p. 559.
23. A. S. Tetelman and A. J. McEvily: *Fracture of Structural Materials.* p. 441, J. Wiley and Sons, New York, 1967.
24. J. M. McHardy and E. H. Hollingsworth: U. S. Navy Bureau of Naval Weapons Cont. NOw 65-0327f, final Report (1966).